Am J Transl Res 2026;18(5):4234-4247
www.ajtr.org /ISSN:1943-8141/AJTR0172462

Original Article

Effect of *Ligilactobacillus salivarius*-derived exosomes on the cariogenicity of *Streptococcus mutans*

Dairen Jiang, Yan Liang

Department of Endodontics, Affiliated Stomatological Hospital of Guizhou Medical University, Guiyang 550000, Guizhou, China

Received March 6, 2026; Accepted April 19, 2026; Epub May 15, 2026; Published May 30, 2026

Abstract: Objective: This study aimed to investigate the effect of exosomes derived from *Ligilactobacillus salivarius* (L.s-Exo) on the cariogenic potential of *Streptococcus mutans* (*S. mutans*) and the underlying metabolic mechanism. Methods: L.s-Exo were isolated by ultracentrifugation and characterized using TEM, NTA, and western blot. *S. mutans* metabolites after L.s-Exo treatment were profiled by GC-MS, and differential pathways were annotated using KEGG. Cariogenic-related phenotypes and acid-stress responses were measured. Results: L.s-Exo displayed exosomal characteristics. Metabolomics revealed widespread metabolic perturbations. L.s-Exo impaired acid tolerance, increased ion leakage, suppressed acid production and glycolytic rate, reduced water-soluble/insoluble EPS, and inhibited biofilm formation. Under acid stress, L.s-Exo elevated proton permeability and decreased cell dry weight, H^+-ATPase activity, and intracellular Pi, accompanied by downregulation of key virulence and glycolysis/acid-production genes. Conclusion: L.s-Exo inhibits *S. mutans* cariogenicity by disrupting metabolic networks and suppressing key virulence gene expression, supporting its use as an anti-caries agent.

Keywords: *Ligilactobacillus salivarius*, exosomes, *Streptococcus mutans*, cariogenicity, metabolomics

Introduction

Dental caries are one of the most prevalent oral infectious diseases worldwide, posing a significant threat to the oral health of all age groups [1]. The pathogenesis of dental caries is closely associated with oral microecological imbalance, among which *Streptococcus mutans* (*S. mutans*) is recognized as the primary cariogenic pathogen [2]. Studies have shown that *S. mutans* can metabolize dietary carbohydrates to produce large amounts of organic acids, leading to a decrease in oral pH and subsequent enamel demineralization [3], and it also synthesizes extracellular polysaccharides (EPS) to form dense biofilms, which not only enhance bacterial adhesion and colonization on tooth surfaces but also create a localized acidic microenvironment conducive to the survival and proliferation of cariogenic bacteria [4]. Additionally, *S. mutans* has evolved efficient acid tolerance mechanisms, with membrane-bound H^+-ATPase playing a crucial role in maintaining intracellular pH homeostasis, enabling it to survive in acidic environments and sustain its cariogenic activity [5, 6].

Traditional caries prevention and treatment methods have limitations in regulating oral microecological balance and avoiding drug resistance [7]. Probiotic-based intervention strategies have gradually emerged as a research focus [8]. *Ligilactobacillus salivarius* (L. salivarius), a commensal probiotic in the oral cavity and intestines, has been proven to exert significant anti-caries effects [9]. Previous studies have demonstrated that *L. salivarius* can inhibit the formation of symbiotic biofilms composed of *S. mutans* and Candida albicans, reduce acid production by *S. mutans*, and interfere with its metabolic processes through secreted metabolites [10]. These metabolites regulate oral microflora balance and reduce cariogenicity by inhibiting key glycolytic enzymes, decreasing EPS synthesis, blocking bacterial adhesion sites, and even disrupting the acid tolerance mechanisms of *S. mutans* [11].

In recent years, bacterial extracellular vesicles (BEVs), nanoscale membrane vesicles secreted by bacteria, have become important mediators of intercellular communication and microeco-

https://doi.org/10.62347/NQWI2760

logical regulation [12]. Unlike mammalian cell-derived exosomes that function primarily in immune regulation and tissue repair, BEVs carry a variety of bioactive molecules, enabling them to modulate bacterial interactions, regulate metabolic pathways, and influence biofilm formation [13]. In the field of oral health, BEVs have shown promising potential for caries prevention and treatment. They can regulate the growth and metabolism of oral microorganisms to maintain microecological balance, participate in immune regulation to enhance the host's defense against cariogenic pathogens, and even serve as targeted drug delivery systems [14]. However, research on the inhibition of *S. mutans* cariogenicity by L. salivarius-derived exosomes (L.s-Exo) is still in its infancy, and their underlying molecular mechanisms remain unclear.

Therefore, this study aimed to isolate and identify exosomes derived from L. salivarius, and to explore their regulatory effects on the cariogenicity of *S. mutans* through a combination of non-targeted metabolomics and in vitro experiments. It is expected to provide a new theoretical basis and experimental support for the development of probiotic-derived exosome-based caries prevention and treatment.

Materials and methods

Culture of Ligilactobacillus salivarius

De Man, Rogosa and Sharpe (MRS) medium (Hangzhou Baisi Biotechnology Co., Ltd.) was prepared. Lyophilized strains (ATCC11741, Shanghai Conservation and Microbiology Center) were taken out of the refrigerator, equilibrated to room temperature, and resuspended in sterile normal saline in a biosafety cabinet (BAKER, USA) with gentle shaking to form a bacterial suspension. The suspension was then inoculated into liquid MRS medium using a sterile inoculation loop. The inoculated medium was anaerobically cultured at 37°C for 48 h, during which the turbidity of the medium was observed regularly. Single colonies were picked and transferred to fresh MRS medium.

Culture of S. mutans

Brain Heart Infusion (BHI) medium (Hangzhou Baisi Biotechnology Co., Ltd.) was prepared. The strain was inoculated into liquid BHI medium in a biosafety cabinet and anaerobically cultured at 37°C for 24 h. Single colonies were selected for 2-3 passages to restore the optimal growth state. For short-term storage, the strain was kept at 4°C; for long-term storage, it was cryopreserved in 50% glycerol at -80°C.

Ultracentrifugation method

Ligilactobacillus salivarius was inoculated into MRS medium and anaerobically cultured at 37°C for 24 h. The bacterial culture was centrifuged at 2000×g for 30 min at 4°C to remove bacterial pellets, then centrifuged at 10,000×g for 45 min at 4°C to eliminate large vesicles. The supernatant was filtered through a 0.45 μm cellulose acetate membrane, and the filtrate was ultracentrifuged at 100,000×g for 70 min at 4°C. The supernatant was discarded, and the L. salivarius-derived exosome (L.s-Exo) pellet was retained and stored at -80°C.

Transmission electron microscopy (TEM)

10 μL of L.s-Exo suspension was dropped onto a carbon-coated copper grid. After 1 min of adsorption, excess liquid was blotted off with filter paper. 10 μL of 2% uranyl acetate was added for staining for 1 min, and residual stain was blotted off with filter paper. The grid was air-dried at room temperature for 15 min, and TEM imaging was performed at an accelerating voltage of 80 kV.

Nanoparticle tracking analysis (NTA)

10 μL of L.s-Exo suspension was diluted to 30 μL with PBS. After the instrument was calibrated with standard particles and verified to be qualified, the diluted L.s-Exo sample was loaded. The instrument automatically detected and recorded the particle size distribution and concentration of L.s-Exo.

BCA assay

Protein standard solutions were diluted with PBS to a final concentration of 0.5 mg/mL to prepare a series of standard solutions. BCA working solution was prepared by mixing reagent A and reagent B at a volume ratio of 50:1. 200 μL of BCA working solution was added to each well, followed by incubation at 37°C for 30 min. The absorbance at 562 nm was measured using a microplate reader (BioTek Epoch, USA),

and the protein concentration was calculated based on the standard curve.

Western blot

Whole-cell proteins of *L. salivarius* were extracted, and acrylamide gel (sodium dodecyl sulfate-polyacrylamide gel electrophoresis, SDS-PAGE) was prepared. A PVDF membrane of the corresponding size was cut and soaked in TBST buffer containing 5% non-fat milk for blocking at room temperature for 2 h. Primary antibodies (1:1000, anti-TSG101 antibody; 10427-2-AP, anti-Calnexin antibody; Wuhan Sanying Biotechnology Co., Ltd.) and secondary antibody were diluted according to the antibody instructions. Band quantitative analysis was performed using ImageJ software.

Untargeted metabolomic

Gas chromatography- mass spectroscopy (GC-MS) was used to measure the metabolic profiles of *S. mutans* before and after L.s-Exo treatment. Metabolomic data were processed using CD and KEGG databases, and bubble plots, bar charts, volcano plots, and box plots were generated.

Experimental grouping

S. mutans was randomly divided into a control group (*S. mutans* alone) and an experimental group (*S. mutans*+L.s-Exo). L.s-Exo was added at a protein concentration of approximately 30 μg/mL. In the co-culture system, the volume ratio of L.s-Exo to *S. mutans* was 1:9, and the culture time was set to 12-48 h [15]. The pH of the medium was adjusted to 3.5, 5.0, and 7.0 to simulate strongly acidic, moderately acidic, and neutral environments, respectively.

Bacterial growth capacity under different pH conditions

The growth capacity of *S. mutans* under acidic stress was evaluated by viable cell counting. BHI liquid media with pH values ranging from 2.5 to 7.0 at 0.5 intervals were prepared. *S. mutans* was inoculated into the above media respectively and anaerobically cultured at 37°C for 3 h. The bacterial culture was serially diluted and spread on BHI agar plates, followed by anaerobic culture at 37°C for 48 h. The number of viable colonies was counted under a microscope.

Potassium ion (K^+) leakage

K^+ leakage was measured to assess bacterial membrane damage under acidic stress using a Potassium (K) Test Kit (Nanjing Jiancheng Bioengineering Institute, C001-1-1). *S. mutans* in the control group and experimental group were inoculated into fresh BHI medium at pH 5.5 (acidic group) and pH 7.3 (neutral control group) respectively, and anaerobically cultured at 37°C for 48 h. A blank group (500 μL deionized water), a standard group (500 μL 0.4 mmol/L K^+ standard solution), and a sample group (500 μL bacterial supernatant) were set up. 2 mL of reagent II was added to each group, and the mixtures were vortexed and incubated at room temperature for 5 min. With deionized water as the blank control, the absorbance at 440 nm was measured using a spectrophotometer, and the K^+ concentration of each group was calculated based on the standard curve.

Mg^{2+} content

Mg^{2+} content was determined using a Magnesium (Mg) test kit (Abcam, Ab102506). *S. mutans* was cultured in BHI medium at pH 5.5 and pH 7.3 for 48 h as described above. An appropriate amount of cell lysis buffer was added to the washed bacterial pellet, and intracellular Mg^{2+} was released by ultrasonic lysis. A blank group (10 μL deionized water), a standard group (10 μL 1.5 mmol/L Mg^{2+} standard solution), and a sample group (10 μL bacterial lysis supernatant) were set up. The absorbance at 540 nm was measured using a spectrophotometer, and the intracellular Mg^{2+} concentration was calculated based on the standard curve.

Acid production capacity

Liquid media containing different carbon sources were prepared by adding 3% (w/v) glucose, sucrose, or fructose (Guangzhou Nuokang Biotechnology Co., Ltd., A085-1-1) to BHI medium, and the initial pH was adjusted to 7.3. 500 μL of *S. mutans* culture was inoculated into the carbon source media. After anaerobic culture at 37°C for 12 h, the final pH of the medium was measured.

Glycolytic capacity

S. mutans in the control group and experimental group were anaerobically cultured at 37°C for 1 h, centrifuged at 8000 rpm for 10 min,

and the bacterial pellet was resuspended in a buffer containing 50 mM KCl and 1 mM $MgCl_2$. The OD_{600} value of the bacterial suspension was adjusted to be consistent, and the pH was titrated to 7.2 with KOH. A curve was plotted with time as the abscissa and pH as the ordinate. The minimum pH reached within 30 min was defined as the glycolytic minimum pH [16].

EPS production

The anthrone-sulfuric acid method was used to quantify water-soluble EPS (WS-EPS) and water-insoluble EPS (WI-EPS) produced by *S. mutans*. Since EPS synthesis is closely associated with the dynamic process of *S. mutans* biofilm development, three representative time points were selected for WI-EPS and WS-EPS determination. 3 h was chosen to represent the initial adhesion stage, 12 h to represent the exponential growth stage, and 20 h to represent the late biofilm maturation stage. *S. mutans* were inoculated into fresh BHI medium and anaerobically cultured at 37°C for 16 h, then diluted 1:20 into 100 mL of fresh BHI medium and cultured for another 3 h until the mid-log growth phase. The absorbance at 620 nm was measured using a microplate reader, and a standard curve was plotted with glucose standard solution to calculate the EPS content.

Crystal violet staining

BHI liquid medium containing 3% sucrose was added, and *S. mutans* suspensions in the control group and experimental group were inoculated at a volume ratio of 1:9. 100 μL of 0.1% (w/v) crystal violet solution was added to each well for staining at room temperature for 20 min. The staining solution was discarded, and the wells were rinsed three times with PBS and dried at room temperature for 30 min. 200 μL of 95% ethanol was added to each well to dissolve the crystal violet, and the absorbance at OD 600 nm was measured using a microplate reader to quantify the biofilm formation [17].

Bacterial dry weight

S. mutans was anaerobically cultured at 37°C for 24 h, and the bacterial culture was transferred to a pre-weighed centrifuge tube. The centrifuge tube containing the washed bacteria was placed in an oven at 105°C and dried to a constant weight. The centrifuge tube was cooled to room temperature in a desiccator, and the total weight of the tube and dried bacteria was accurately weighed using an analytical balance. Calculation: Dry weight of bacteria = Total weight - Pre-weighed weight of empty centrifuge tube.

Hydrogen-ATPase (H^+-ATPase) activity

H^+-ATPase activity was determined using the H^+-ATPase Kit (Nanjing Jiancheng Bioengineering Institute, A095-1-2). Standard samples were serially diluted to prepare a series of standard solutions for drawing a calibration curve. 50 μL of chromogenic reagent A and 50 μL of chromogenic reagent B were added to each well, followed by gentle oscillation and color development at 37°C for 15 min in the dark. 50 μL of stop solution was added to each well to terminate the reaction. With the blank well as the control, the absorbance at 450 nm was measured using a microplate reader within 15 min. A calibration curve was plotted based on the absorbance of the standard solutions, and the H^+-ATPase activity of the sample was calculated and multiplied by the dilution factor to obtain the actual activity.

Inorganic phosphate (Pi) content

Pi content was determined using a Phosphorus (Pi) Test Kit (Nanjing Jiancheng Bioengineering Institute, C006-1-1). 200 μL of cell lysis buffer was added to the bacterial pellet, and intracellular Pi was released by ultrasonic lysis. After centrifugation, the supernatant was collected as the sample solution for Pi detection. A series of Pi standard solutions were added to 25 mL stoppered colorimetric tubes, supplemented with water to the marked line and mixed thoroughly. 1 mL of ammonium molybdate-sulfuric acid mixed reagent was added to each tube, and the absorbance at 690 nm was measured using a spectrophotometer. A standard curve was plotted with Pi concentration as the ordinate and absorbance as the abscissa.

qRT-PCR

Total RNA of *S. mutans* was extracted using the Trizol method (Thermo Fisher Scientific, 15596018CN). cDNA was synthesized using the PrimeScript™ RT reagent kit with gDNA Eraser (Thermo Fisher Scientific, RR047A). qRT-

Table 1. Primer sequences

Primer	Primer (5'-3')	Sequence
gtfB-F	*Forward*	AATCACGGCCACTCCTGAAG
gtfB-R	*Reverse*	TCAAGCCATGCGCAATCAAC
vicK-F	*Forward*	TGAGCAGGCATTGGAGT
vicK-R	*Reverse*	TTTCACGGCGGTTTAAG
comD-F	*Forward*	AGTTCTGACTTGTTTAGGCG
comD-R	*Reverse*	CGTTTTTTGACCTTCATCTT
luxS-F	*Forward*	AGCCCCTTATGTCCGTC
luxS-R	*Reverse*	AACAGTCAATCATCCCGTC
F-ATPase-F	*Forward*	CGGATGCGTGTTGCTCTTACTG
F-ATPase-R	*Reverse*	CCTGCTTGATGTTGATGTTGGC
ldh-F	*Forward*	GCTGATGTTGCCGTTGTTGA
ldh-R	*Reverse*	CCGTTGATGTTGCCGTTGTA
pfkA-F	*Forward*	ATGACGGTGAAGGTGATGGA
pfkA-R	*Reverse*	TCCATCACCTTCACCGTCAT
eno-F	*Forward*	GGATGAAGCTGAAGGTGATG
eno-R	*Reverse*	CATCACCTTCAGCTTCATCC
16S rRNA-F	*Forward*	AGAGTTTGATCCTGGCTCAG
16S rRNA-R	*Reverse*	GGTTACCTTGTTACGACTTC

PCR was performed on a real-time PCR instrument using TB Green® Premix Ex Taq™ II (Thermo Fisher Scientific, RR820A). The relative expression level of target genes was calculated using the $2^{-\Delta\Delta Ct}$ method, with the control group as the calibrator. The primer sequences are listed in **Table 1**.

Statistical analysis

All experiments were repeated 3 times. Data were expressed as mean ± SD. Statistical analysis was performed using SPSS 19.0 software, and the independent samples t-test was used for comparison of means between groups. A *P*-value < 0.05 was considered significant.

Results

Characterization of L.s-derived exosomes

TEM was employed to observe the microstructure of L.s-Exo. TEM images showed that L.s-Exo isolated by ultracentrifugation exhibited the typical morphologic characteristics of exosomes, namely a bilayer membrane and a cup-shaped structure (**Figure 1A**). To further verify the observation results, NTA was performed to measure the particle size of L.s-Exo. The results showed that the average particle size of L.s-Exo isolated by ultracentrifugation was 77.9 nm, which was consistent with the structural features of L.s-Exo observed by TEM (**Figure 1B**). In addition, the western blot results demonstrated that L.s-Exo expressed the exosome-positive marker TSG101, while Calnexin, an exosome-negative marker, was not detected (**Figure 1C**). TSG101 was expressed in the L.s-Exo fraction but not in *L. salivarius* cells, which should be interpreted as vesicle-specific enrichment rather than cellular expression. Therefore, the absence of TSG101 in the bacterial lysate does not contradict its detection in L.s-derived exosomes; instead, this further indicates that the isolated vesicles possessed characteristic exosomal protein cargo and were not substantially contaminated by whole-cell components. Collectively, these results confirm that the L.s-Exo isolated by ultracentrifugation in this experiment conform to the standard characteristics of exosomes.

Effects of L.s-Exo on the metabolic profile of S. mutans revealed by untargeted metabolomics

Untargeted metabolomics analysis was performed on the co-culture system of L.s-Exo and *S. mutans* to investigate the changes in metabolic pathways and differential metabolites. The pathway bubble plot showed that the most significantly affected metabolic pathways included tropane, piperidine, and pyridine alkaloid biosynthesis, flavonoid biosynthesis, and ABC transporters (**Figure 2A**), among which ABC transporters are closely associated with *S. mutans* cariogenicity. The pathway bar plot further verified the enrichment trend of the above pathways and also revealed that taurine and hypotaurine metabolism, glutathione metabolism and other pathways were also significantly regulated (**Figure 2B**). In the volcano plot of differential metabolites, red, blue and gray dots represented significantly up-regulated, down-regulated and non-significantly differential metabolites, respectively, and the size of the dots was positively correlated with the VIP value (**Figure 2C**). The box plot of the ATP metabolic pathway indicated that L.s-Exo could significantly enhance the ATP metabolic activity of *S.*

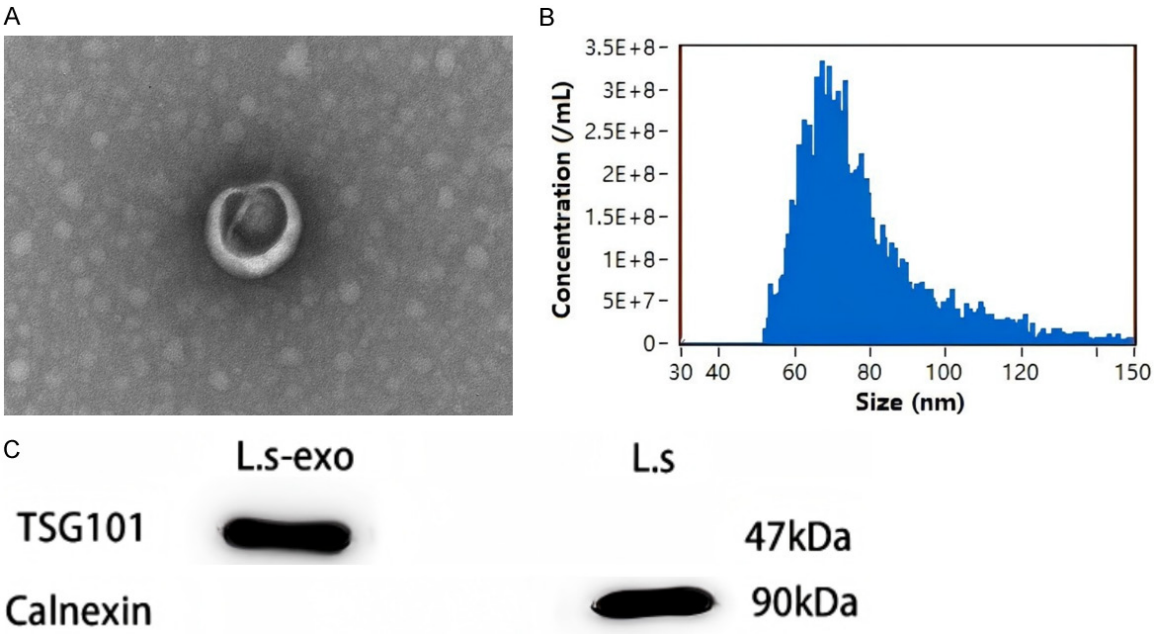

Figure 1. Identification of *Ligilactobacillus salivarius*-derived exosomes (L.s-Exo). A. Microstructure of L.s-Exo observed by transmission electron microscopy (TEM) (scale bar corresponds to 100 nm); B. Particle size distribution of L.s-Exo analyzed by nanoparticle tracking analysis (NTA); C. Expression of characteristic proteins of L.s-Exo detected by western blot. All experiments were performed in triplicate (n=3), and representative images are shown.

mutans (**Figure 2D**). These results showed that L.s-Exo plays a pivotal role in reshaping the metabolic network of *S. mutans*.

Effects of L.s-Exo on the growth and acid damage tolerance of S. mutans

The growth of both the *S. mutans* group (control group) and the *S. mutans*+L.s-Exo group (experimental group) was pH-dependent. The *S. mutans* group reached the peak of viable cell count at pH 5.5, while the optimal growth pH of the *S. mutans*+L.s-Exo group shifted to pH 6.0 (a neutral shift). Additionally, the viable cell count of the *S. mutans*+L.s-Exo group was significantly lower than that of the *S. mutans* group under all pH conditions tested (**Figure 3A**). In an acidic environment, both *S. mutans* and *S. mutans*+L.s-Exo released magnesium and potassium ions into the culture medium. The release of potassium ions in the *S. mutans*+L.s-Exo group was significantly higher than that in the *S. mutans* group (**Figure 3B**), and the release of magnesium ions in the *S. mutans*+L.s-Exo group was significantly higher than that in the *S. mutans* group (**Figure 3C**), suggesting that L.s-Exo could significantly enhance the bacterial cell damage of *S. mutans* under acidic conditions.

Inhibitory effects of L.s-Exo on acid production and glycolysis capacity of S. mutans

Both *S. mutans* and *S. mutans*+L.s-Exo produced acid after 12 h of cultivation in BHI medium with sucrose, fructose and glucose as carbon sources, and the acid production of the *S. mutans*+L.s-Exo group was significantly lower than that of the *S. mutans* group. The pH difference between the two groups was the largest in sucrose medium, followed by glucose and the smallest in fructose (**Figure 4A**, **4B**). *In vitro* glycolysis assay showed that both *S. mutans* and *S. mutans*+L.s-Exo could rapidly metabolize substrates to produce acid, resulting in a decrease in the pH of the system. However, at all time points within the first 30 min, the pH value of the *S. mutans* group was significantly lower than that of the *S. mutans*+L.s-Exo group, and the glycolytic acid production rate of *S. mutans* was significantly higher than that of the intervention group (**Figure 4C**), suggesting that L.s-Exo could directly inhibit the glycolytic acid production process of *S. mutans*.

L.s-Exo inhibits exopolysaccharide synthesis and biofilm formation in S. mutans

Results from the anthrone method assay showed that the production of water-soluble

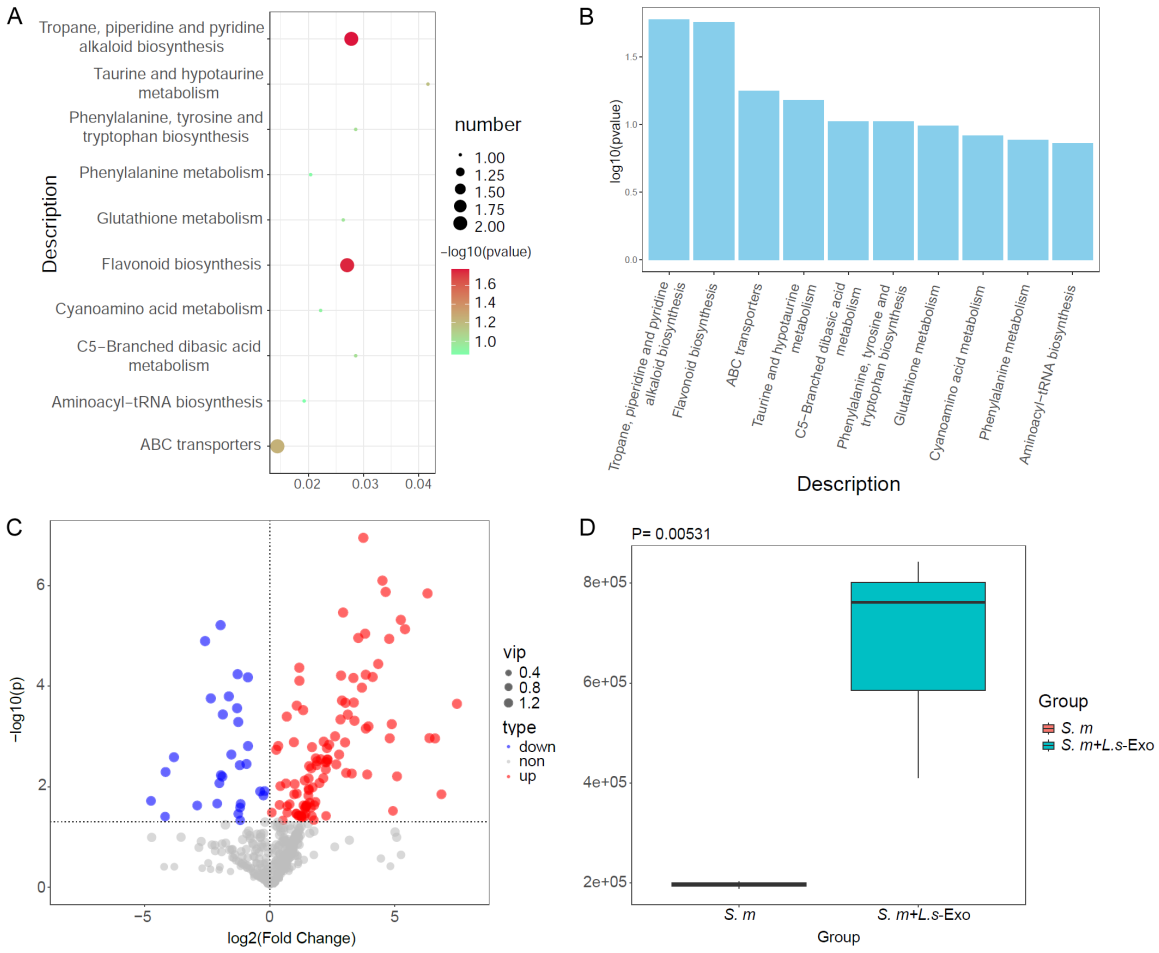

Figure 2. Untargeted metabolomic analysis. A. Bubble plot of metabolic pathway enrichment; B. Bar plot of metabolic pathway enrichment; C. Volcano plot of differential metabolites; D. Box plot of the adenosine triphosphate (ATP) metabolic pathway. All experiments were performed in triplicate (n=3).

glucans (WSG) and water-insoluble glucans (WIG) in the *S. mutans* group was significantly higher than that of the *S. mutans*+L.s-Exo group at the early (3 h), middle (12 h) and late (20 h) stages of biofilm formation. Moreover, this inhibitory effect persisted throughout the entire process of biofilm formation (**Figure 5A**, **5B**). Quantitative detection by crystal violet staining demonstrated that biofilm in the *S. mutans*+L.s-Exo group was significantly lower than that of the *S. mutans* group after 12 h of cultivation (**Figure 5C**), suggesting that L.s-Exo could significantly inhibit the adhesion and formation of *S. mutans* biofilm.

Regulation of L.s-Exo on cell membrane permeability and expression of related functional genes in S. mutans

Proton permeability assay showed that the system pH of the *S. mutans*+L.s-Exo group was significantly higher than that of the *S. mutans* group (**Figure 6A**). The results of bacterial dry weight detection revealed that the bacterial dry weight of the *S. mutans*+L.s-Exo group was significantly lower than that of the *S. mutans* group (**Figure 6B**). The activity of H^+-ATPase in the *S. mutans*+L.s-Exo group was significantly lower than that of the *S. mutans* group (**Figure 6C**). Inorganic phosphorus determination indicated that the Pi release of the *S. mutans*+L.s-Exo group was significantly lower than that of the *S. mutans* group at 10 min and 20 min of cultivation, with the difference still existing but reduced at 60 min (**Figure 6D**). Quantitative real-time PCR analysis demonstrated that the mRNA expression levels of *gtfB, comD*, *vicK*, *F-ATPase* and *LuxS* in *S. mutans* were significantly down-regulated after L.s-Exo intervention (**Figure 6E**), suggesting that L.s-Exo modulates the cell membrane permeability of *S.*

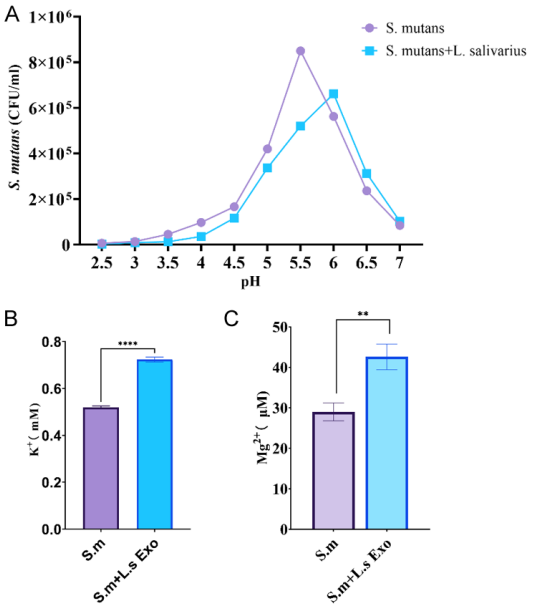

Figure 3. Growth and acid damage tolerance of *S. mutans* intervened by L.s-Exo. A. Growth ability of *S. mutans* under different pH conditions; B. Potassium ion (K^+) concentration in the culture medium after 48 h of co-culture; C. Magnesium ion $(Mg^2)^+$ concentration in the culture medium after 48 h of co-culture. All experiments were performed in triplicate (n=3). $^{**}P < 0.01$, $^{****}P < 0.0001$.

mutans, reduces its biomass and H^+-ATPase activity, exerts a time-dependent inhibition on Pi release, and downregulates the expression of key cariogenic genes.

L.s-Exo downregulates the expression of core genes related to glycolysis/acid production in S. mutans

To investigate further the molecular mechanism underlying the inhibitory effect of L.s-Exo on acid production and glycolytic capacity of *S. mutans*, qRT-PCR analysis revealed that the expression levels of ldh, pfkA, and peno were significantly downregulated after L.s-Exo intervention (**Figure 7A-C**), with the expression of ldh being the most markedly suppressed. These results indicated that L.s-Exo inhibits the glycolysis and acid production of *S. mutans* by targeting the downregulation of core genes in the glycolytic pathway, which constitutes an important molecular basis for its inhibitory effect on the acid-producing capacity of *S. mutans*.

Discussion

As a pivotal approach for elucidating microbial interactions, untargeted metabolomics analysis in this study identified three core metabolic pathways closely associated with the cariogenicity of *S. mutans*, namely the ABC transporter pathway, aromatic amino acid metabolic pathway, and glutathione metabolic pathway. These findings provide crucial evidence for clarifying the anti-caries mechanism of L.s-Exo from the perspective of metabolic regulation.

TSG101, a key component of the endosomal sorting complex required for transport (ESCRT), is directly involved in exosome biogenesis and selectively enriched in exosomal membranes or lumens, serving as a reliable positive marker [18]. In contrast, Calnexin is an endoplasmic reticulum-resident protein and is typically excluded from exosomes, thus it is used as a negative control to rule out contamination from intracellular organelles [19]. The specific detection of TSG101 and absence of Calnexin in L.s-Exo not only confirm the successful isolation of exosomes but also validate the purity of the sample, which is a prerequisite for subsequent functional experiments.

The ABC transporter pathway plays multiple critical roles in the cariogenic process of *S. mutans*. It not only participates in the secretion and degradation of EPS, directly modulating the structural compactness and hydraulic resistance of biofilms [20], but also enhances the adherence capacity of *S. mutans* to tooth surfaces and the efficiency of biofilm formation by regulating the transport of capsular polysaccharides and the expression of bacterial surface adhesion structures [21, 22]. Previous studies have confirmed that certain ABC transporter genes can be co-expressed with virulence genes and mediate the cascade regulation of cariogenic phenotypes through two-component signal systems (TCS) [23, 24]. comD is one of the core components of the Two-Component Signal Transduction System (TCSTS) comDE in *S. mutans* [25]. vicK is a histidine kinase gene of the VicRKX two-component signal transduction system in *S. mutans* [26]. In this study, after L.s-Exo treatment, the EPS synthesis of *S. mutans* was significantly reduced, and the expression of *vicK* and *comD* genes was downregulated. These results suggest that L.s-Exo may attenuate the biofilm-forming ability of *S. mutans* by interfering with this pathway and its downstream signal transduction.

Dysregulation of the aromatic amino acid metabolic pathway also provides an important explanation for the anti-caries effect of L.s-Exo.

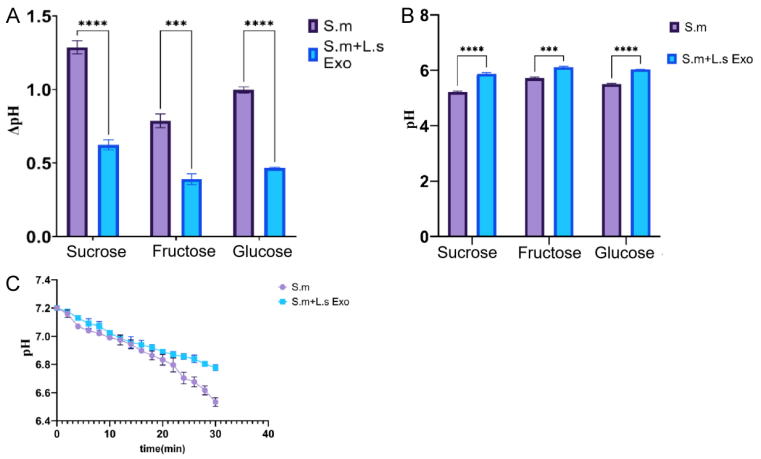

Figure 4. Effects of L.s-Exo on acid production and glycolysis capacity of *S. mutans*. A. Delta pH (ΔpH) values under different carbon sources after 12 h of co-culture; B. Medium pH values under different carbon sources after 12 h of co-culture; C. Changes in the system pH value over time in the *in vitro* glycolysis assay. All experiments were performed in triplicate (n=3). $^{***}P < 0.001$, $^{****}P < 0.0001$.

Metabolites of tryptophan can specifically bind to quorum-sensing proteins of *S. mutans*, thereby downregulating the transcriptional level of biofilm-related genes [27, 28]. Tyrosine can reduce the cell surface hydrophobicity of bacteria and interfere with their initial adhesion process [29]. In addition, metabolites of phenylalanin can not only significantly inhibit the formation of dual-species biofilms of *S. mutans* and *Candida albicans*, but also interfere with the synthesis of AI-2 signaling molecules and disrupt the quorum-sensing regulatory mechanism [30, 31]. In the oral microenvironment, phenylacetic acid produced by *S. mutans* through phenylalanine metabolism can form a local acidic microenvironment to promote enamel demineralization, yet excessive metabolism generates cytotoxicity that exerts a self-limiting effect on the bacterial population size [32]. In the L.s-Exo treatment group of this study, the sugar utilization efficiency of *S. mutans* was decreased and biofilm formation ability was impaired, indicating that L.s-Exo can regulate the production of metabolites by this pathway to inhibit cariogenic phenotypes.

Regulation of the glutathione metabolic pathway is involved in the modulation of *S. mutans* cariogenicity by affecting EPS synthesis. Glutathione S-transferase (GST), encoded by the gst gene, not only participates in bacterial detoxification but also plays a key role in oxidative stress regulation and signal transduction [33, 34]. Furthermore, glutathionylation can directly regulate the activity of transcription factors such as VicR and GcrR, thereby inhibiting the expression of EPS synthesis-related genes including *gtfB/C* and *gbpB/C*, and ultimately attenuating biofilm formation ability [35, 36]. *gtfB* are core caries-associated genes of *S. mutans*. Belonging to the glucosyltransferases (Gtfs) gene family, they collectively mediate sucrose-dependent EPS synthesis, and serve as the key molecular basis for bacterial biofilm formation and cariogenicity [37, 38]. In this study, after L.s-Exo intervention, the expression level of the *gtfB* gene in *S. mutans* was significantly downregulated, the contents of both WIG and WSG were reduced synchronously, and the biofilm structure became loose. These results confirm that L.s-Exo can target this pathway to affect EPS synthesis and destroy the structural stability of biofilms.

As the core structure for *S. mutans* to exert its cariogenicity, the biofilm takes EPS as the matrix skeleton and integrates polysaccharides, proteins, nucleic acids, and other components. It endows bacteria with the ability to resist host immunity and exogenous antimicrobial agents, and simultaneously maintains an acidic microenvironment within the biofilm to accelerate enamel demineralization [4, 39]. Biofilm formation by *S. mutans* relies on two major pathways, sucrose-dependent and sucrose-independent. The sucrose-dependent pathway is mediated by members of the glucosyltransferase (GTFs) family, which provides energy and an adhesion basis for biofilms [21, 40, 41]. Gene knockout experiments have confirmed that deletion of *gtfB/C/D* leads to a significant reduction in the cariogenicity of *S. mutans* [42, 43]. In this study, the contents of WIG and WSG in the L.s-Exo co-culture group were both significantly decreased, accompanied by the downregulation of the *gtfB* gene. These findings directly verify that L.s-Exo can destroy the material basis of biofilm formation

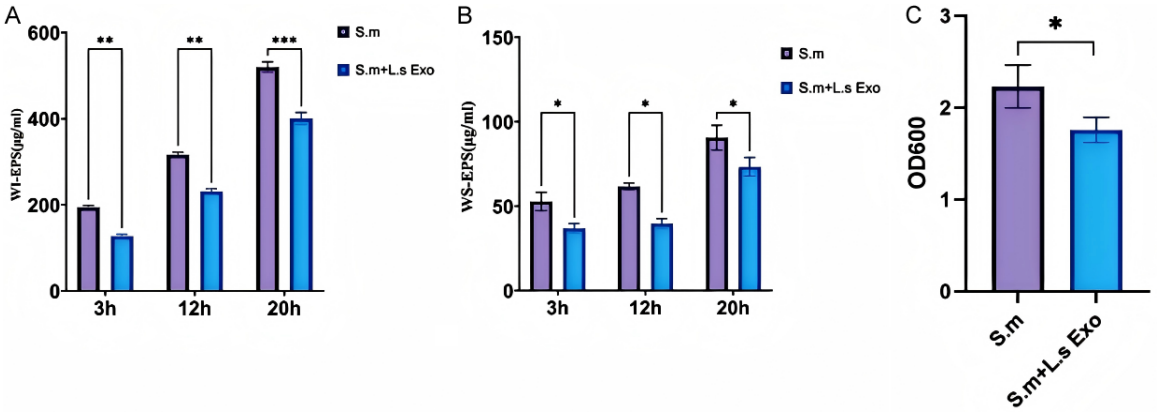

Figure 5. Effects of L.s-Exo on exopolysaccharide synthesis and biofilm formation of *S. mutans*. A. Water-insoluble EPS (WI-EPS) production at different time points; B. Water-soluble EPS (WS-EPS) production at different time points; C. Quantitative results of crystal violet staining for biofilm after 12 h. All experiments were performed in triplicate (n=3). $^{*}P < 0.05$, $^{**}P < 0.01$, $^{***}P < 0.001$.

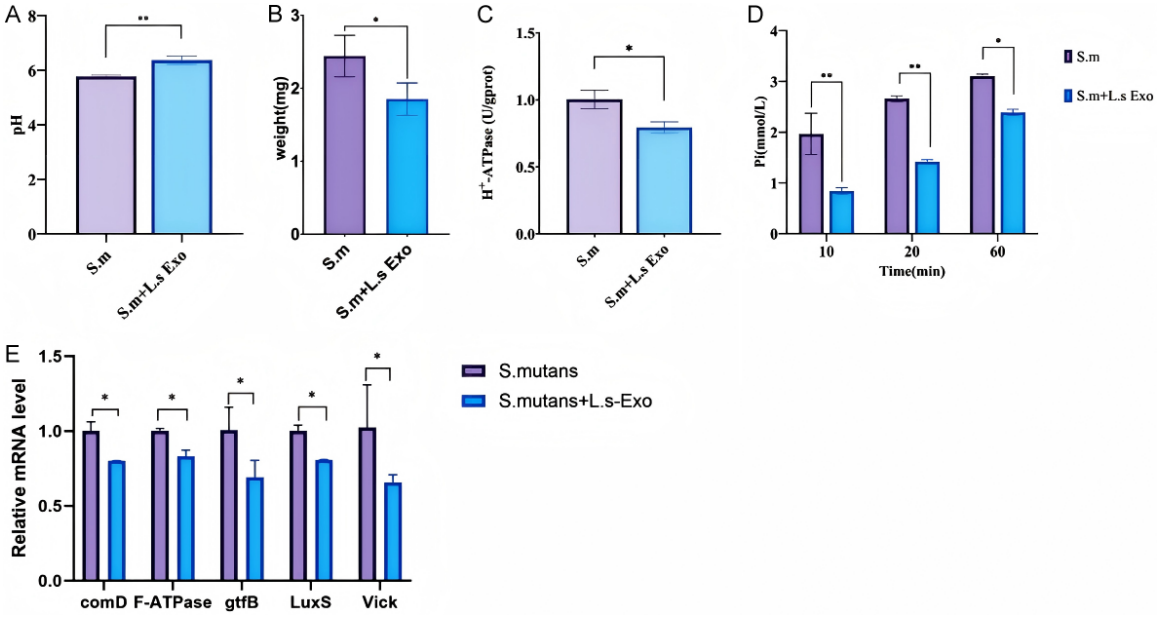

Figure 6. L.s-Exo regulates membrane permeability and functional gene expression in *S. mutans*. A. Results of cell membrane proton permeability assay; B. Results of bacterial dry weight detection; C. Results of H^+-ATPase activity assay; D. Inorganic phosphorus (Pi) release at different time points; E. Relative mRNA expression levels of cariogenic-related genes. All experiments were performed in triplicate (n=3). $^{*}P < 0.05$, $^{**}P < 0.01$.

by inhibiting the expression of key genes involved in EPS synthesis.

TCS and quorum-sensing systems play a central role in the regulation of *S. mutans* biofilm formation. Experiments on comC, comD, comE and comX gene-deficient strains constructed by researchers [44] have shown that the signaling pathways involving these genes are essential for normal biofilm formation, and knockout of any single gene results in abnormal biofilm structure. In addition, the LuxS gene, a key gene for AI-2 signaling molecule synthesis, when deleted, accelerates the production of water-insoluble glucans, affects biofilm formation and sugar metabolism regulation [45, 46]. In this study, the expression levels of *gtfB*, *comD*, *vicK*, *LuxS* and other genes were all significantly downregulated after L.s-Exo intervention, indicating that L.s-Exo can block the regu-

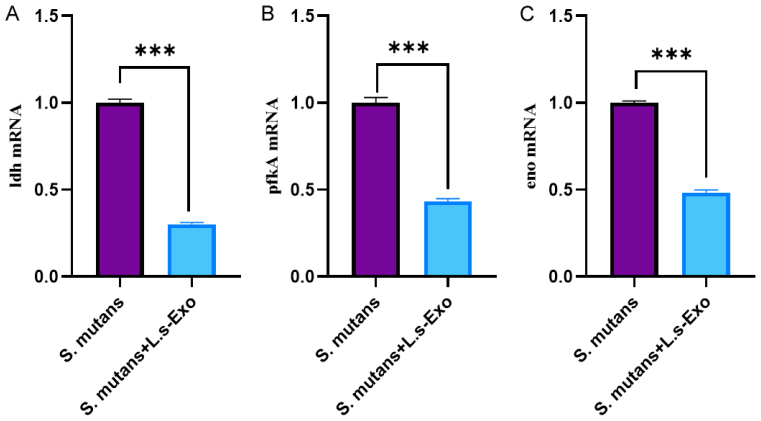

Figure 7. L.s-Exo downregulates the mRNA expression of glycolysis/acid production core genes in *S. mutans*. A-C. The relative mRNA expression levels of ldh, pfkA, eno in the *S. mutans* group and *S. mutans*+L.s-Exo group were detected by qRT-PCR, with 16S rRNA as the reference gene. All experiments were performed in triplicate (n=3). $^{***}P < 0.001$.

latory network of biofilm formation at the molecular level by interfering with the signal transduction of TCS and quorum-sensing systems.

Acid tolerance is a core characteristic that enables *S. mutans* to survive in the acidic oral microenvironment and exert its cariogenicity, which mainly relies on membrane-bound proton-translocating ATPase (F-ATPase/H^+-ATPase) to maintain intracellular pH homeostasis [47, 48]. This enzyme drives proton efflux through ATP hydrolysis to maintain the transmembrane pH gradient (ΔpH), enabling the maintenance of a near-neutral intracellular state even in a low-pH extracellular environment. It thus protects the activity of key glycolytic enzymes and ensures continuous acid production and metabolism of bacteria [47, 49]. However, in this study, L.s-Exo intervention led to a significant decrease in the activity of H^+-ATPase in *S. mutans*, which directly impairs its proton efflux capacity. It is speculated that this change causes intracellular H^+ accumulation, disrupts acid-base balance, and ultimately reduces the survival ability of bacteria in acidic environments. In addition, L.s-Exo also specifically downregulates the expression of core genes in glycolysis pathway, directly inhibiting the glycolysis process of *S. mutans* and reducing the synthesis of lactic acid, which further explains its inhibitory effect on the acid production capacity of *S. mutans* from the molecular level.

Notably, the metabolomic data of this study showed an increase in the activity of ATP-related metabolic pathways in *S. mutans* after L.s-Exo treatment. This phenomenon seems contradictory to the decreased H^+-ATPase activity but actually reflects a compensatory metabolic change in bacteria. Due to the inhibited function of H^+-ATPase, ATP cannot be normally consumed for proton efflux, leading to a transient intracellular accumulation of ATP. This further results in a 'false positive' elevation of activity in activity detected by metabolomics [50, 51], rather than an actual enhancement of bacterial energy production. This finding further confirms that L.s-Exo can specifically target H^+-ATPase, interfere with the energy metabolism distribution of *S. mutans*, and indirectly inhibit its acid tolerance and cariogenicity.

The innovation of this study lies in focusing on the emerging research direction of *Ligilactobacillus salivarius*-derived exosomes, and systematically revealing the mode of action of L.s-Exo in inhibiting *S. mutans* cariogenicity through regulating metabolic pathways, interfering with biofilm formation mechanisms, and targeting key acid-tolerance enzymes. It fills the gap in the current research on the anti-caries mechanism of probiotic exosomes and provides a new theoretical basis for probiotic intervention strategies for dental caries.

This study had certain limitations. First, the research was conducted only in an *in vitro* monoculture system of *S. mutans*, without considering the interactions of the complex oral microbial flora. The anti-caries effect of L.s-Exo in a multi-species microecosystem needs to be further verified. Second, the specific active components of L.s-Exo responsible for the anti-caries effect have not been identified, which limits its subsequent application and transformation. Third, there was a lack of animal model and clinical research data, and the *in vivo* anti-caries effect, optimal administration method and safety of L.s-Exo remain to be explored. Future research aims to further explore the key molecular targets and pathway networks of L.s-Exo in regulating *S. mutans* cariogenicity thr-

ough multi-omics approaches, and clarify the upstream and downstream regulatory relationships. In addition, the active components of L.s-Exo will be isolated and purified to identify the core anti-caries substances and explore their specific mechanisms of action, so as to provide a more comprehensive basis for its application in clinical prevention and treatment of dental caries.

Disclosure of conflict of interest

None.

Address correspondence to: Yan Liang, Department of Endodontics, Affiliated Stomatological Hospital of Guizhou Medical University, No. 9 Beijing Road, Guiyang 550000, Guizhou, China. E-mail: Ss1023cc@163.com

References

[1] Kaur P, Vyas M and Sharma S. Dental caries: unveiling the state-of-the-art insights and crafting hypotheses for oral health. Curr Pharm Des 2024; 30: 2667-2670.

[2] Zhou Y, Zhang C, Deng Y, Lei L and Hu T. Oral microecological community- Streptococcus mutans dysbiosis and interaction provide therapeutic perspectives for dental caries. Arch Oral Biol 2025; 178: 106367.

[3] Lin Y, Chen J, Zhou X and Li Y. Inhibition of Streptococcus mutans biofilm formation by strategies targeting the metabolism of exopolysaccharides. Crit Rev Microbiol 2021; 47: 667-677.

[4] Klein MI, Hwang G, Santos PH, Campanella OH and Koo H. Streptococcus mutans-derived extracellular matrix in cariogenic oral biofilms. Front Cell Infect Microbiol 2015; 5: 10.

[5] Sasaki Y, Nogami E, Maeda M, Nakanishi-Matsui M and Iwamoto-Kihara A. A unique F-type H^+-ATPase from Streptococcus mutans: an active H^+ pump at acidic pH. Biochem Biophys Res Commun 2014; 443: 677-82.

[6] Ziogas M, Drummond I, Todorovic I, Kraczkowsky K, Han Y, Zhang H, Wu H and Spatafora G. SloR-SRE binding to the S. mutans mntH promoter is cooperative. J Bacteriol 2025; 207: e0047024.

[7] Warreth A. Dental caries and its management. Int J Dent 2023; 2023: 9365845.

[8] Vonaesch P, Garneau JR and Dominguez-Bello MG. From global to local: rethinking the design of probiotic intervention strategies. Trends Microbiol 2026; 34: 390-405.

[9] Staszczyk M, Jamka-Kasprzyk M, Kościelniak D, Cienkosz-Stepańczak B, Krzyściak W and Jurczak A. Effect of a short-term intervention with Lactobacillus salivarius probiotic on early childhood caries-an open label randomized controlled trial. Int J Environ Res Public Health 2022; 19: 12447.

[10] Zeng Y, Fadaak A, Alomeir N, Wu TT, Rustchenko E, Qing S, Bao J, Gilbert C and Xiao J. Lactobacillus plantarum disrupts S. mutans-C. albicans cross-kingdom biofilms. Front Cell Infect Microbiol 2022; 12: 872012.

[11] Zhang MD, Cheng XQ and Xu X. Latest findings on polyketides/non-ribosomal peptides that are secondary metabolites of Streptococcus mutans. Sichuan Da Xue Xue Bao Yi Xue Ban 2023; 54: 685-691.

[12] Zhou Z, Sun L, Tu Y, Yang Y, Hou A, Li J, Luo J, Cheng L, Li J, Liang K and Yang J. Exploring naturally tailored bacterial outer membrane vesicles for selective bacteriostatic implant coatings. Adv Sci (Weinh) 2024; 11: e2405764.

[13] Nie X, Li Q, Chen X, Onyango S, Xie J and Nie S. Bacterial extracellular vesicles: vital contributors to physiology from bacteria to host. Microbiol Res 2024; 284: 127733.

[14] Leiva-Sabadini C, Berríos P, Saavedra P, Carrasco-Rojas J, González-Aramundiz JV, Vera M, Tarifeño-Saldivia E, Schuh CMAP and Aguayo S. Biofilm formation on collagen substrates modulates Streptococcus mutans bacterial extracellular nanovesicle production and cargo. Nanoscale Adv 2025; 7: 5670-5680.

[15] Jiang S, Huang XJ, Zhang CF, Cai ZY and Zou T. Morphological and proteomic analyses of the biofilms generated by Streptococcus mutans isolated from caries-active and caries-free adults. J Dent Sci 2015; 10: 206-215.

[16] Belli WA and Marquis RE. Catabolite modification of acid tolerance of Streptococcus mutans GS-5. Oral Microbiol Immunol 1994; 9: 29-34.

[17] Santiago B, MacGilvray M, Faustoferri RC and Quivey RG Jr. The branched-chain amino acid aminotransferase encoded by ilvE is involved in acid tolerance in Streptococcus mutans. J Bacteriol 2012; 194: 2010-9.

[18] Greening DW, Xu R, Ji H, Tauro BJ and Simpson RJ. A protocol for exosome isolation and characterization: evaluation of ultracentrifugation, density-gradient separation, and immunoaffinity capture methods. Methods Mol Biol 2015; 1295: 179-209.

[19] Tu M, Liu AM, Huang W, Wang D, Chen HQ and Hu XY. Macrophages-derived small extracellular vesicles regulate chondrocyte proliferation and affect osteoarthritis progression via upregulating osteopontin expression. J Cell Commun Signal 2025; 19: e70008.

[20] Sadaoka N, Le MN-T, Kawada-Matsuo M, Eng S, Zendo T, Nakanishi J, Takeda K, Shiba H and Komatsuzawa H. Opposing genetic polymorphisms of two ABC transporters contribute to

the variation of nukacin resistance in Streptococcus mutans. Appl Environ Microbiol 2024; 90: e0208423.
[21] Zhang Q, Ma Q, Wang Y, Wu H and Zou J. Molecular mechanisms of inhibiting glucosyltransferases for biofilm formation in Streptococcus mutans. Int J Oral Sci 2021; 13: 30.
[22] Moon J, Seo K and Kwon JS. Novel two-stage expansion of Streptococcus mutans biofilm supports EPS-targeted prevention strategies for early childhood caries. NPJ Biofilms Microbiomes 2025; 11: 65.
[23] Desmond P, Best JP, Morgenroth E and Derlon N. Linking composition of extracellular polymeric substances (EPS) to the physical structure and hydraulic resistance of membrane biofilms. Water Res 2018; 132: 211-221.
[24] Fisher ML, Allen R, Luo Y and Curtiss R 3rd. Export of extracellular polysaccharides modulates adherence of the cyanobacterium synechocystis. PLoS One 2013; 8: e74514.
[25] Milly TA, Engler ER, Chichura KS, Buttner AR, Koirala B, Tal-Gan Y and Bertucci MA. Harnessing multiple, nonproteogenic substitutions to optimize CSP: comD hydrophobic interactions in group 1 Streptococcus pneumoniae. Chembiochem 2021; 22: 1940-1947.
[26] Deng Y, Yang Y, Zhang B, Chen H, Lu Y, Ren S, Lei L and Hu T. The vicK gene of Streptococcus mutans mediates its cariogenicity via exopolysaccharides metabolism. Int J Oral Sci 2021; 13: 45.
[27] Yan Q, Rogan CJ, Pang YY, Davis EW 2nd and Anderson JC. Ancient co-option of an amino acid ABC transporter locus in pseudomonas syringae for host signal-dependent virulence gene regulation. PLoS Pathog 2020; 16: e1008680.
[28] Yang XY, Liao XH, Ye J, Shao C, Wang B and Liu Y. Effects of D-tryptophan on biofilm formation and dispersal in Streptococcus mutans. Tianjin Medical Journal 2016; 44: 1199.
[29] Paul P, Chakraborty P, Sarker RK, Chatterjee A, Maiti D, Das A, Mandal S, Bhattacharjee S, Dastidar DG and Tribedi P. Tryptophan interferes with the quorum sensing and cell surface hydrophobicity of Staphylococcus aureus: a promising approach to inhibit the biofilm development. 3 Biotech 2021; 11: 376.
[30] Brandenburg KS, Rodriguez KJ, McAnulty JF, Murphy CJ, Abbott NL, Schurr MJ and Czuprynski CJ. Tryptophan inhibits biofilm formation by pseudomonas aeruginosa. Antimicrob Agents Chemother 2013; 57: 1921-5.
[31] Paul P, Roy R, Das S, Sarkar S, Chatterjee S, Mallik M, Shukla A, Chakraborty P and Tribedi P. The combinatorial applications of 1,4-naphthoquinone and tryptophan inhibit the biofilm formation of Staphylococcus aureus. Folia Microbiol (Praha) 2023; 68: 801-811.
[32] Bosken YK, Ai R, Hilario E, Ghosh RK, Dunn MF, Kan SH, Niks D, Zhou H, Ma W, Mueller LJ, Fan L and Chang CA. Discovery of antimicrobial agent targeting tryptophan synthase. Protein Sci 2022; 31: 432-442.
[33] Mazari AMA, Zhang L, Ye ZW, Zhang J, Tew KD and Townsend DM. The multifaceted role of glutathione S-transferases in health and disease. Biomolecules 2023; 13: 688.
[34] Samsri S, Kortheerakul C, Kageyama H and Waditee-Sirisattha R. Molecular and biochemical characterization of a plant-like iota-class glutathione S-transferase from the halotolerant cyanobacterium Halothece sp. PCC7418. J Appl Microbiol 2024; 135: lxae230.
[35] Ren Z, Chen L, Li J and Li Y. Inhibition of Streptococcus mutans polysaccharide synthesis by molecules targeting glycosyltransferase activity. J Oral Microbiol 2016; 8: 31095.
[36] Aloke C, Onisuru OO and Achilonu I. Glutathione S-transferase: a versatile and dynamic enzyme. Biochem Biophys Res Commun 2024; 734: 150774.
[37] Setiawan AS, Subarnas A, Djais AA, Milanda T and Ichwan SJA. Psidium guajava leaves n-Hexane fraction antibacterial activity and the inhibition of gene expression of gtfB and gtfC in the combination Streptococcus mutans ATCC 25175 and Veillonella parvula ATCC 10790T. J Exp Pharmacol 2025; 17: 639-650.
[38] Wang R, Wang Y, Lei Z, Hao L and Jiang L. Glucosyltransferase-modulated Streptococcus mutans adhesion to different surfaces involved in biofilm formation by atomic force microscopy. Microbiol Immunol 2022; 66: 493-500.
[39] Gao Z, Chen X, Wang C, Song J, Xu J, Liu X, Qian Y and Suo H. New strategies and mechanisms for targeting Streptococcus mutans biofilm formation to prevent dental caries: a review. Microbiol Res 2023; 278: 127526.
[40] Rezaei T, Mehramouz B and Gholizadeh P. Factors associated with Streptococcus mutans pathogenicity in the oral cavity. Biointerface Res Appl Chem 2023; 13.
[41] Lemos JA, Palmer SR, Zeng L, Wen ZT, Kajfasz JK, Freires IA, Abranches J and Brady LJ. The biology of Streptococcus mutans. Microbiol Spectr 2019; 7: 10.1128.
[42] Wang R, Deng L, Lei Z, Wu P, Wang Y, Hao L, Li T and Jiang L. Nanoscale adhesion forces of glucosyltransferase B and C genes regulated Streptococcal mutans probed by AFM. Mol Oral Microbiol 2020; 35: 49-55.
[43] Lynch DJ, Michalek SM, Zhu M, Drake D, Qian F and Banas JA. Cariogenicity of Streptococcus mutans glucan-binding protein deletion mu-

tants. Oral Health Dent Manag 2013; 12: 191-9.
[44] Li YH, Tang N, Aspiras MB, Lau PC, Lee JH, Ellen RP and Cvitkovitch DG. A quorum-sensing signaling system essential for genetic competence in Streptococcus mutans is involved in biofilm formation. J Bacteriol 2002; 184: 2699-708.
[45] Deng Z, Hou K, Valencak TG, Luo XM, Liu J and Wang H. AI-2/LuxS quorum sensing system promotes biofilm formation of lactobacillus rhamnosus GG and enhances the resistance to enterotoxigenic escherichia coli in germ-free zebrafish. Microbiol Spectr 2022; 10: e0061022.
[46] Kanthenga HT, Banicod RJS, Ntege W, Njiru MN, Javaid A, Tabassum N, Kim YM and Khan F. Functional diversity of AI-2/LuxS system in lactic acid bacteria: impacts on biofilm formation and environmental resilience. Res Microbiol 2025; 176: 104296.
[47] Matsui R and Cvitkovitch D. Acid tolerance mechanisms utilized by Streptococcus mutans. Future Microbiol 2010; 5: 403-17.
[48] Zhu W, Liu S, Zhuang P, Liu J, Wang Y and Lin H. Characterization of acid-tolerance-associated small RNAs in clinical isolates of Streptococcus mutans: potential biomarkers for caries prevention. Mol Med Rep 2017; 16: 9242-9250.
[49] Baker JL, Faustoferri RC and Quivey RG Jr. Acid-adaptive mechanisms of Streptococcus mutans-the more we know, the more we don't. Mol Oral Microbiol 2017; 32: 107-117.
[50] Sasaki M, Kodama Y, Shimoyama Y, Ishikawa T and Kimura S. Aciduricity and acid tolerance mechanisms of Streptococcus anginosus. J Gen Appl Microbiol 2018; 64: 174-179.
[51] Magalhães PP, Paulino TP, Thedei G Jr and Ciancaglini P. Kinetic characterization of P-type membrane ATPase from Streptococcus mutans. Comp Biochem Physiol B Biochem Mol Biol 2005; 140: 589-97.